Proceedings of the International Conference on Industrial Engineering and Operations Management

Publisher: IEOM Society International, USA DOI: 10.46254/AF07.20260092
Published: May 13, 2026

Experimental and Kinetic Study of CO_2 Absorption in a NaOH Spray Dryer System

Lawrence Koech, Kasturie Premlall, Douw Faurie and Brilliant Vunene Chauke
Tshwane University of Technology
Department of Chemical, Metallurgical and Materials Engineering
Private Bag X680, Pretoria, 0001, Republic of South Africa
KoechLK@tut.ac.za

Abstract

This study investigates the removal of CO_2 from a gas mixture using sodium hydroxide in a laboratory-scale spray dryer. A gas stream containing 1.4% v/v CO_2 was treated with aqueous NaOH solutions at concentrations of 3 wt.%, 7 wt.%, and 9 wt.%. The study evaluated the impact of inlet gas temperatures ranging from 140°C to 170°C and aqueous solution flow rates between 21 ml/min and 39.6 ml/min. Gas-phase CO_2 at the dryer outlet was monitored and used to fit a time-dependent apparent first-order model fitted directly to the integrated solution by nonlinear least squares. The two-parameter model predicted the reaction rate with high R^2 (0.97–0.99). Higher inlet gas temperature and increased aqueous solution flow rate improved CO_2 removal under the tested conditions, and an intermediate NaOH concentration (7 wt.%) gave the best performance. Kinetic analysis returned an activation energy of 41.57 kJ/mol for the initial uptake term (K_1), while the decay term (K_2) showed weak temperature dependence with an activation energy of 3.13 kJ/mol. These findings show the feasibility of using spray drying technology for carbon capture while providing essential kinetic parameters for process scaling.

Keywords
Spray drying, sodium hydroxide, CO_2 capture, kinetic modelling, reaction rate, Arrhenius equation.

1. Introduction

Global warming has gained worldwide attention due to unpredictable changes in the climate system observed since the mid-20th century. These changes include rising atmospheric temperatures, rising sea levels, and a decrease in the amount of snow and ice (Hu et al., 2018). Atmospheric carbon dioxide (CO_2) is recognised as the most influential greenhouse gas contributing to these effects. The concentration of this gas has increased from a pre-industrial level of 280 parts per million (ppm) to over 400 ppm currently (Mahmoudkhani and Keith, 2009). This is primarily caused by the burning of fossil fuels in the commercial, industrial, and transportation sectors (Chen et al., 2005; Lee et al., 2008). International concern over climate change has led to the adoption of strict rules and regulations to limit emissions. Participating countries like South Africa adopted the Kyoto Protocol at the Earth Summit in 1997 and the Paris Agreement in 2015, intending to reduce greenhouse gas emissions and achieve net-zero by 2050 (Chen et al., 2005; UNDP, 2025). To prevent dangerous shifts in the global climate, scientific roadmaps suggest that atmospheric concentrations must be kept below 550 ppm (Lee et al., 2011). Achieving this requires a global average emission rate below 0.055 kg of carbon per kilowatt hour (kWh) by the latter half of the 21st century (Lee et al., 2008). Many countries are now making a great effort to implement these mitigation strategies and meet international targets.

Carbon capture, utilisation, and storage (CCUS) is currently considered the most promising technological approach to achieve carbon neutrality (Cai et al., 2025; Zhou et al., 2022). Mitigation efforts generally target large fixed point sources of emissions, such as power stations, oil refineries, and steel works (Mahmoudkhani and Keith, 2009). Post-combustion capture is popular because it allows the continued use of cheap and abundant fossil fuels while

substantially reducing emissions. Another emerging technology is direct air capture, which removes the gas from ambient air to manage dispersed emissions from sectors like aviation (Hu et al., 2018; Rodríguez-Mosqueda et al., 2018).

One major challenge in carbon capture is the low concentration of the gas in the atmosphere, which requires processing very large volumes of air. This necessitates the use of contactors with large surface areas that can operate with a very low pressure drop (Rodríguez-Mosqueda et al., 2018; Stolaroff et al., 2008). Standard industrial solvents like amines often require high amounts of energy for recovery and are susceptible to degradation and high volatility (Yoo et al., 2013). Aqueous systems also face the challenge of significant water loss through evaporation, which can be as high as 20 moles of water per mole of gas captured, depending on the humidity and temperature (Stolaroff et al., 2008).

Various sorbent types have been used to trap the gas, including chemical solvents and solid powders. Amine-based solvents like monoethanolamine are currently the most common commercial option, though they are corrosive and energy intensive (Yoo et al., 2013). Sodium hydroxide solutions are an attractive alternative because they have a higher absorption capacity and are much cheaper and more abundant than amines (Stolaroff et al., 2008; Yoo et al., 2013). Solid sorbents such as calcium oxide, lithium-based ceramics, and sodium zirconate are also under investigation (Bamiduro et al., 2017; Cai et al., 2025; Zhou et al., 2022). Lithium orthosilicate is a leading high-temperature candidate due to its fast sorption kinetics and high sequestration capacity (Hu et al., 2018).

Laboratory-scale spray dryer systems have been tested to evaluate CO_2 removal efficiency under different operating conditions. A study by Chen et al. (2005) showed that the best removal efficiency for a spray dryer using a mixture of sodium hydroxide and calcium hydroxide reached 48% at an operating temperature of 150 ℃. The study also demonstrated that the removal efficiency increases with higher absorbent concentrations and lower inlet gas concentrations. A study by Tavan and Hosseini (2017) indicated that efficiency increases when using a smaller nozzle diameter, 0.5 mm instead of 1 mm, because it creates a larger surface area for the droplets to contact the gas. Chen et al. (2005) identified operating temperatures of around 100 to 150℃ as optimal for sodium hydroxide systems, whereas other absorbents like diethanolamine are not as effective at these high temperatures because of reverse reactions. Studies on sodium hydroxide sprays in open towers suggest that this method can produce a large surface area for absorption while avoiding the cost of packing material (Mahmoudkhani and Keith, 2009; Stolaroff et al., 2008).

The spray drying process is significant because it provides high removal efficiency without producing wastewater (Chen et al., 2005; Tavan and Hosseini, 2017). This system atomises the liquid into tiny droplets, which creates a large surface area that promotes rapid chemical reactions. Unlike packed towers, spray dryers can operate with a smaller pressure drop and lower liquid to gas ratios, which reduces reagent consumption (Chen et al., 2005; Troyano et al., 2020). Spray drying is a well-established industrial technique, meaning it is easily scalable for commercial mass production of capture materials and is an energy-efficient technology for mitigating carbon emissions.

This study aimed to evaluate the effect of key operational parameters (absorbent concentration, inlet gas temperature, and aqueous solution flow rate) on the CO_2 capture performance of a spray dryer.

2. Methodology

2.1 Materials and preparation of NaOH aqueous solution

Sodium hydroxide pellets (>97% purity) were sourced from Labchem, South Africa, while 99% CO_2 cylinder gas was sourced from Afrox, South Africa. NaOH aqueous solution was prepared by weighing the required mass of NaOH and dissolved in distilled water in a volumetric flask, then mixed with a magnetic stirrer until the solution was homogeneous.

2.1 Experimental procedure

Experiments were carried out on a laboratory-scale spray dryer (MSD/EV) shown in Figure 1. The system comprised the spray chamber, nozzle and pump, heated gas supply, product collector and a CO_2 analyser. A gas mixture was produced by metering CO_2 from a cylinder, regulated with a rotameter, into the ambient air stream to achieve an inlet CO_2 concentration of 1.4% v/v used throughout the study. The inlet gas mixture was heated with an electrical heater on the spray dryer to the required temperature and the temperature was monitored at the spray chamber inlet and outlet.

Before each run, the heater and gas flow were stabilised. When a steady inlet/outlet temperature was achieved, NaOH aqueous solution was pumped to the two-fluid nozzle and atomised with the spray gas. Droplets evaporated and reacted with CO_2 in the gas stream, forming dry solids which were collected at the chamber base and cyclone. CO_2 concentration at the gas outlet was recorded continuously by an ETG MCA100 analyser. This process was repeated while varying the experimental conditions such as inlet gas temperature (140 – 180°C), NaOH concentration (3 - 9wt.%), and aqueous solution flow rate (21 – 40 ml/min). Each experiment was allowed to proceed up to 180 seconds, where an equilibrium reading for CO_2 at the exit was achieved. Each experiment was also conducted in triplicate, and the average was recorded to ensure reproducibility.

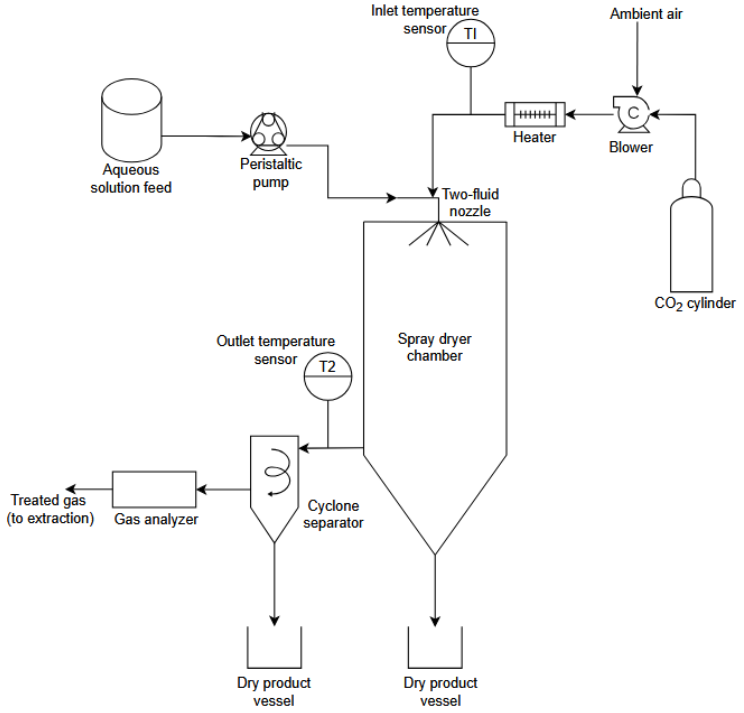

Figure 1. Laboratory-scale spray drying setup

2.1. Reaction rate modelling and non-linear parameter estimation

The gas-phase CO_2 concentration was analysed using a time-dependent apparent reaction rate model. The approach accounts for the progressive reduction in effective reaction capacity caused by droplet evaporation and changing gas–liquid contact during spray drying (Tavan and Hosseini, 2017). The gas-phase CO_2 mole fraction, $y(t)$, was assumed to follow a first-order decay with a time-dependent rate coefficient shown in equation (1).

$$\frac{dy}{dt} = -k(t)y(t) \qquad \text{Equation 1}$$

Where the apparent rate coefficient decreases exponentially with time

$$k(t) = K_1 \exp(-K_2 t) \qquad \text{Equation 2}$$

Substituting into the rate equation (equation 1)

$$\frac{dy}{dt} = -K_1 \exp(-K_2 t) y(t) \qquad \text{Equation 3}$$

Integrating equation 3 becomes

$$y(t) = y0 \; exp\left[-\frac{K_1}{K_2}(1 - \exp(-K_2 t))\right] \qquad \text{Equation 4}$$

Where $y0$ is the initial CO_2 mole fraction at the start of the experiment, and K_1 and K_2 are kinetic parameters to be calculated (Tavan and Hosseini, 2017).

The kinetic parameters K_1 and K_2 were estimated using non-linear least-squares regression implemented in Python via *scipy.optimize.curve_fit* function. To ensure physical consistency, the parameters were constrained to positive values using the Trust Region Reflective (TRF) algorithm. This method directly fits the integrated model equation to the experimental CO_2 concentration data without numerical differentiation, thereby reducing sensitivity to experimental noise (Hofer et al., 2022). For each experimental temperature, the measured CO_2 mole fraction $y_{exp}(t)$ was fitted by minimising the sum of squared residuals as shown in equation 5.

$$\sum_{i=1}^{N}\left[y_{exp}(t_i) - y_{model}(t_i, K_1, K_2)\right]^2 \qquad \text{Equation 5}$$

Where $y_{model}(t_i, K_1, K_2)$ is given by the integrated model expression (equation 4). K_1 and K_2 are estimated by minimising this expression.

The initial CO_2 mole fraction $y0$ was fixed to the measured value at $t = 0$. Model performance was evaluated using the coefficient of determination (R^2) and root-mean-square error (RMSE) (Chai and Draxler, 2014).

3. Results and discussion

3.1. CO_2 absorption behaviour

3.1.1. Effect of inlet gas temperature

The data in Figure 2 displays the impact of varying the inlet gas temperature between 140°C and 170°C on CO_2 absorption. As the temperature increases, the final concentration of CO_2 at the exit decreases. At a temperature of 170°C, the system reaches an equilibrium concentration of approximately 1.23% within 180 seconds. The lowest temperature (140°C) results in a higher outlet concentration of about 1.31%. This trend is likely due to enhanced evaporation and improved atomisation at higher temperatures being the dominant mechanism, rather than a solubility-driven effect, since the equilibrium solubility of CO_2 typically decreases with increasing temperature. (Diamond and Akinfiev, 2003; Koech et al., 2023).

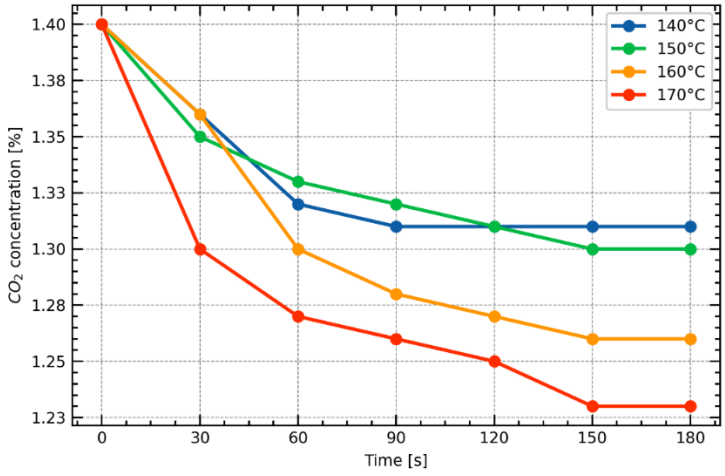

Figure 2. Effect of inlet gas temperature on CO_2 removal

3.1.2. The effect of NaOH concentration

Figure 3 illustrates the effect of NaOH concentration on CO_2 capture performance. Increasing NaOH concentration increases the chemical driving force for CO_2 absorption and enhances the apparent reaction rate within the droplets, resulting in higher removal efficiency. Results indicate that 7% NaOH concentration achieves the best performance, reaching a CO_2 concentration of approximately 1.19% at 170°C. Both the 3% and 9% concentrations show higher final CO_2 levels of 1.23% and 1.22% (respectively). This behaviour indicates that an optimal concentration exists to maximise the reaction between CO_2 and the NaOH solution (where 7% performs better than higher or lower concentrations).

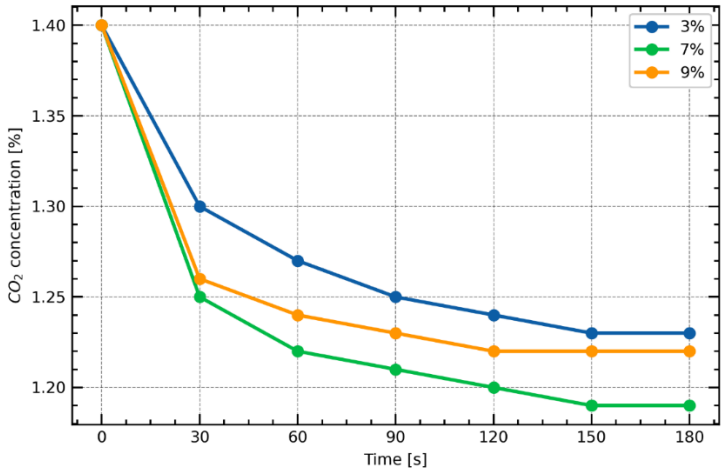

Figure 3. Effect of NaOH concentration on CO_2 removal

3.1.3 Effect of the feed flow rate

Figure 4 presents the relationship between the aqueous solution flow rate and the CO_2 concentration at the exit. An increase in the aqueous solution flow rate from 21 ml/min to 39.6 ml/min leads to a consistent reduction in the outlet CO_2 concentration. The highest flow rate (39.6 ml/min) yields the lowest exit concentration of 1.22%, while the lowest flow rate (21 ml/min) results in approximately 1.28%. These results occur because higher flow rates increase the volume of reactant sprayed into the chamber, which facilitates increased availability of the reactive species between the dispersed droplets and the gas mixture.

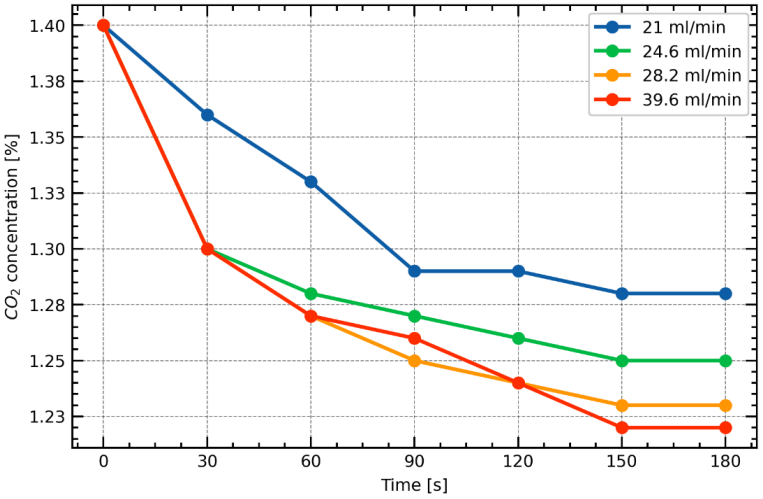

Figure 4. Effect of aqueous solution flow rate on CO_2 removal

3.2 Kinetic parameter estimation

After obtaining the values of K_1 and K_2, the instantaneous apparent reaction rate was calculated as:

$$r(t) = K_1 \exp(-K_2 t)\, y(t) \qquad \text{Equation 6}$$

This expression was used to generate modelled reaction-rate profiles as a function of time as shown in Figure 5. The modelled rates were compared with calculated values and used to assess the effect of temperature on reaction behaviour.

Figure 5 compares calculated apparent reaction rate profiles with modelled profiles from the time-dependent reaction rate model at the four temperatures. The model captures the overall decay trend of CO_2 concentration with time; higher coefficients of determination (R^2) were obtained for the four temperatures. The fitted parameter K_1 represents the initial apparent reaction rate, while K_2 describes the rate at which this apparent reactivity decreases with time due to

droplet drying and loss of effective reaction area (Dahlan et al., 2011; González et al., 2008; Hong et al., 2014). All four temperatures show a fast initial uptake that decays towards a low steady rate, consistent with an initial period of effective gas–liquid contact followed by progressive loss of active liquid surface as droplets dry.

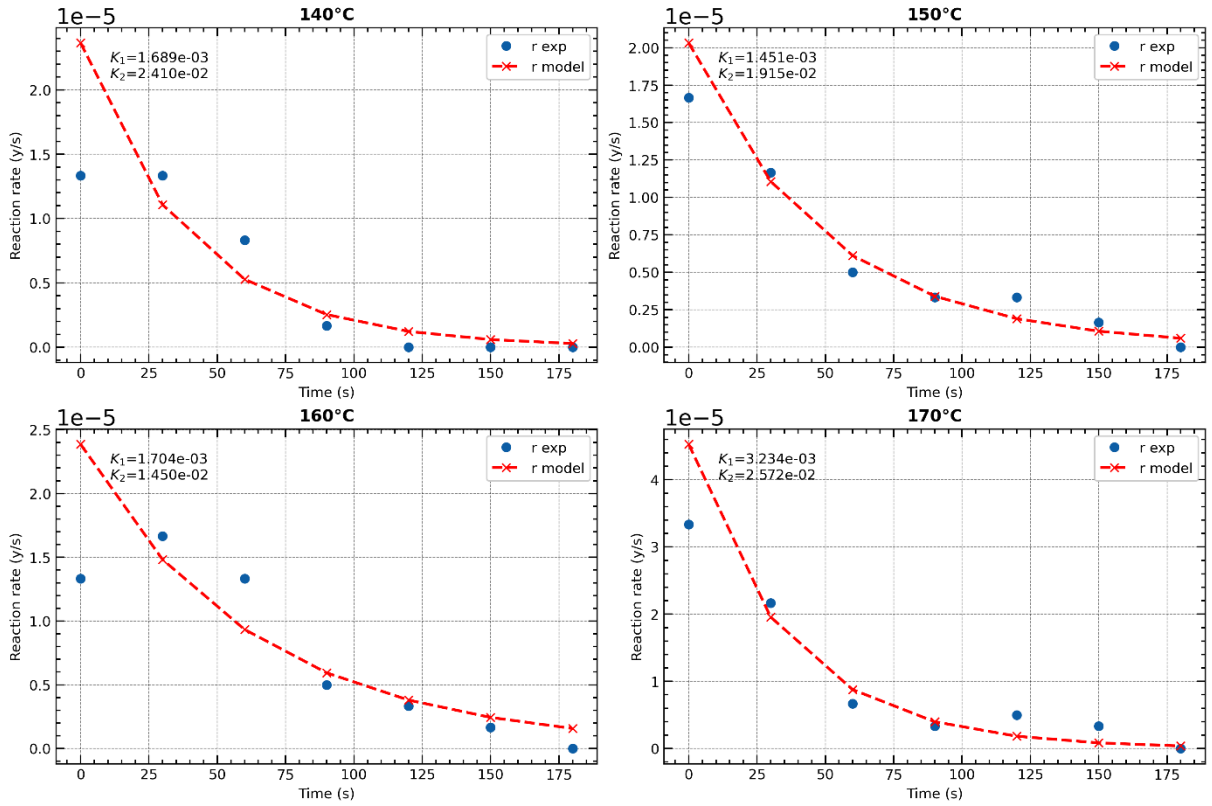

Figure 5. Reaction rate prediction at different temperatures.

The non-linear fit of the integrated two-parameter model (equation 4) yields K_1 and K_2 values that reproduce the reaction rate with R^2 in the range 0.97–0.99 and relative RMSE of 0.2–0.6% of the mean signal (Table 1). The highest K_1 (3.23×10^{-3} s^{-1}) occurs at 170 °C, but this condition also shows the highest decay constant K_2 (2.57×10^{-2} s^{-1}), indicating a strong, short-lived uptake likely driven by faster intrinsic chemistry combined with rapid droplet evaporation. The best prediction is at 150°C ($R^2 = 0.992$, relative RMSE = 0.22%), where the apparent uptake is lower but more sustained, so the two-parameter model matches the measured decay closely. It is also evident from Figure 5 that there are some deviations at early times (first 20 – 40 seconds) for some temperatures. This shows that the model captures the overall decay except for a brief section of the droplets, which is attributed to the fraction of very fine droplets with faster uptake. Studies on single-droplet drying literature show that drying follows stages where surface and internal transport rates change, producing non-uniform time behaviour across a droplet cloud (Gregson et al., 2019). This may not be resolved by the two-parameter model and might require measuring other parameters, such as droplet size, to reduce the deviations.

Table 1. Reaction rate, kinetic parameters, and performance metrics

Temp (°C)	K_1 (s^{-1})	K_2 (s^{-1})	R^2	RMSE	Relative RMSE
140	0.001689	0.024096	0.974393	5.23E-05	0.393032
150	0.001451	0.019146	0.992425	2.87E-05	0.215628
160	0.001664	0.013955	0.978494	7.43E-05	0.569707
170	0.003234	0.025719	0.983789	7.00E-05	0.547904

3.3 Temperature dependence of kinetic parameters

Figure 6 shows Arrhenius plots for the kinetic parameters K_1 and K_2. A clear temperature dependence is observed for K_1, yielding a moderate activation energy, indicating the contribution of chemical reaction steps to the initial apparent CO_2 uptake. K_2 shows weak temperature dependence, indicating that the decay of reaction capacity is largely controlled by physical processes such as droplet evaporation and changes in interfacial area rather than activated chemical reactions.

The Arrhenius analysis shows a clear difference in the temperature sensitivity of the two kinetic parameters. The initial uptake term, K_1, exhibits a strong dependence on temperature, with an activation energy of 41.57 kJ/mol and a pre-exponential factor of 154.98. On the other hand, the decay term, K_2, shows only weak temperature dependence, with an activation energy of 3.13 kJ/mol and a pre-exponential factor of 0.035. Both Arrhenius plots show strong fits (R^2 = 0.99 and 0.98, respectively). This indicates consistent behaviour across the temperature range studied.

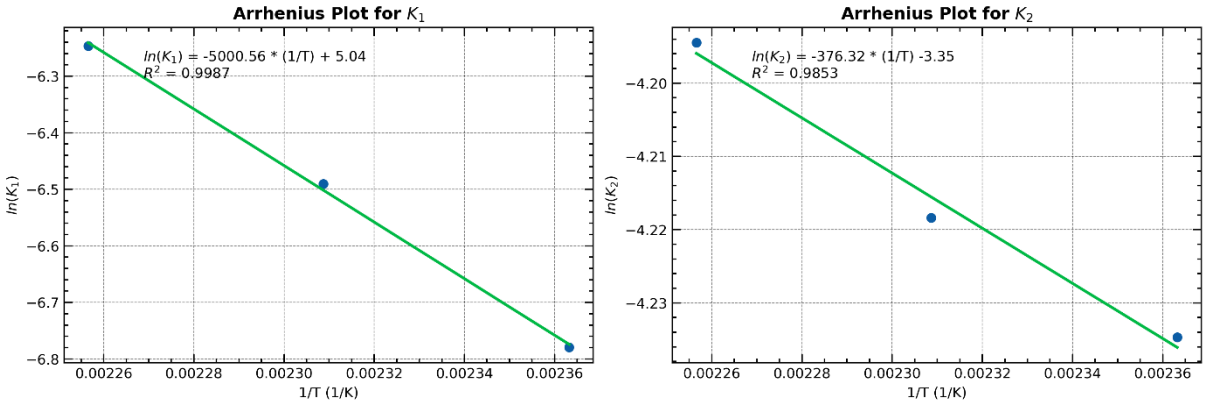

Figure 6. Arrhenius plots for the kinetic parameters K_1 and K_2

4. Conclusion

The study identified the critical parameters influencing the absorption efficiency. Under the conditions tested, increasing inlet gas temperature and increasing aqueous solution flow rate improved CO_2 uptake, while NaOH concentration showed a non-linear effect, with 7 wt.% giving the best removal. The time-dependent apparent first-order model fitted the experimental CO_2 reaction rate, indicating that a two-parameter description captures this behaviour across the tested range. Kinetic parameters from nonlinear regression yield K_1 and K_2 values, which were used to evaluate the Arrhenius equation. Arrhenius analysis gives an activation energy of 41.57 kJ/mol for the initial uptake term (K_1) and 3.13 kJ/mol for the decay term (K_2), confirming that the temperature sensitivity of the initial uptake is larger than that of the decay process. The limitation encountered in this study is the lack of droplet size characterisation and narrow concentration range tested. For precise prediction to be achieved, it is recommended to include supplementary measurements such as droplet size and distribution, droplet and gas temperature profiles within the spray chamber to improve the Arrhenius estimations.

References

Bamiduro, F., Ji, G., Brown, A.P., Dupont, V.A., Zhao, M., Milne, S.J., Spray-Dried Sodium Zirconate: A Rapid Absorption Powder for CO_2 Capture with Enhanced Cyclic Stability. ChemSusChem 10, 2059–2067. 2017. https://doi.org/10.1002/cssc.201700046

Cai, L., Xue, H., Hu, X., Yang, X., Zhang, Y., Constructing structure-stabilized and performance-improved porous Li4SiO4 hollow microspheres via spray-drying process for high-temperature CO2 capture. Separation and Purification Technology 377, 134455. 2025.https://doi.org/10.1016/j.seppur.2025.134455

Chai, T., Draxler, R.R., 2014. Root mean square error (RMSE) or mean absolute error (MAE)? – Arguments against avoiding RMSE in the literature. Geosci. Model Dev. 7, 1247–1250. https://doi.org/10.5194/gmd-7-1247-2014

Chen, J.-C., Fang, G.-C., Tang, J.-T., Liu, L.-P., Removal of carbon dioxide by a spray dryer. Chemosphere 59, 99–105. 2005. https://doi.org/10.1016/j.chemosphere.2004.09.076

Dahlan, I., Lee, K.T., Kamaruddin, A.H., Mohamed, A.R., Sorption of SO2 and NO from simulated flue gas over rice husk ash (RHA)/CaO/CeO2 sorbent: Evaluation of deactivation kinetic parameters. Journal of Hazardous Materials 185, 1609–1613. 2011.https://doi.org/10.1016/j.jhazmat.2010.10.053

Diamond, L.W., Akinfiev, N.N., Solubility of CO2 in water from −1.5 to 100 °C and from 0.1 to 100 MPa: evaluation of literature data and thermodynamic modelling. Fluid Phase Equilibria 208, 265–290. 2003.https://doi.org/10.1016/S0378-3812(03)00041-4

González, B., Grasa, G.S., Alonso, M., Abanades, J.C., Modeling of the Deactivation of CaO in a Carbonate Loop at High Temperatures of Calcination. Ind. Eng. Chem. Res. 47, 9256–9262. 2008.https://doi.org/10.1021/ie8009318

Gregson, F.K.A., Robinson, J.F., Miles, R.E.H., Royall, C.P., Reid, J.P., Drying Kinetics of Salt Solution Droplets: Water Evaporation Rates and Crystallization. J. Phys. Chem. B 123, 266–276. 2019. https://doi.org/10.1021/acs.jpcb.8b09584

Hofer, L.R., Krstajić, M., Smith, R.P., 2022. JAXFit: Trust Region Method for Nonlinear Least-Squares Curve Fitting on the GPU. https://doi.org/10.48550/ARXIV.2208.12187

Hong, Y.S., Zhang, Z.F., Cai, Z.P., Zhao, X.H., Liu, B.S., Deactivation Kinetics Model of H_2 S Removal over Mesoporous $LaFeO_3$ /MCM-41 Sorbent during Hot Coal Gas Desulfurization. Energy Fuels 28, 6012–6018. 2014. https://doi.org/10.1021/ef5008825

Hu, Y., Liu, W., Zhou, Z., Yang, Y., Preparation of Li_4 SiO_4 Sorbents for Carbon Dioxide Capture via a Spray-Drying Technique. Energy Fuels 32, 4521–4527. 2018.https://doi.org/10.1021/acs.energyfuels.7b03051

Koech, L., Rutto, H., Seodigeng, T., Experimental evaluation of lime spray drying for SO_2 absorption. AIMSES 10, 325–340. 2023. https://doi.org/10.3934/environsci.2023019

Lee, J.B., Eom, T.H., Oh, B.S., Baek, J.-I., Ryu, J., Jeon, W.S., Wi, Y.H., Ryu, C.K., CO2 capture from flue gas using potassium-based dry regenerable sorbents. Energy Procedia 4, 1494–1499. 2011.https://doi.org/10.1016/j.egypro.2011.02.016

Lee, J.B., Ryu, C.K., Baek, J.-I., Lee, J.H., Eom, T.H., Kim, S.H., Sodium-Based Dry Regenerable Sorbent for Carbon Dioxide Capture from Power Plant Flue Gas. Ind. Eng. Chem. Res. 47, 4465–4472. 2008. https://doi.org/10.1021/ie0709638

Mahmoudkhani, M., Keith, D.W., Low-energy sodium hydroxide recovery for CO2 capture from atmospheric air—Thermodynamic analysis. International Journal of Greenhouse Gas Control 3, 376–384. 2009. https://doi.org/10.1016/j.ijggc.2009.02.003

Rodríguez-Mosqueda, R., Bramer, E.A., Brem, G., CO2 capture from ambient air using hydrated Na2CO3 supported on activated carbon honeycombs with application to CO2 enrichment in greenhouses. Chemical Engineering Science 189, 114–122. 2018.https://doi.org/10.1016/j.ces.2018.05.043

Stolaroff, J.K., Keith, D.W., Lowry, G.V., Carbon Dioxide Capture from Atmospheric Air Using Sodium Hydroxide Spray. Environ. Sci. Technol. 42, 2728–2735. 2008. https://doi.org/10.1021/es702607w

Tavan, Y., Hosseini, S.H., A novel rate of the reaction between NaOH with CO2 at low temperature in spray dryer. Petroleum 3, 51–55. 2017. https://doi.org/10.1016/j.petlm.2016.11.006

Troyano, J., Çamur, C., Garzón-Tovar, L., Carné-Sánchez, A., Imaz, I., Maspoch, D., Spray-Drying Synthesis of MOFs, COFs, and Related Composites. Acc. Chem. Res. 53, 1206–1217. 2020.https://doi.org/10.1021/acs.accounts.0c00133

UNDP, South Africa | Climate Promise 2025. [WWW Document]. URL https://climatepromise.undp.org/what-we-do/where-we-work/south-africa (accessed 2.5.26).

Yoo, M., Han, S.-J., Wee, J.-H., Carbon dioxide capture capacity of sodium hydroxide aqueous solution. Journal of Environmental Management 114, 512–519. 2013.https://doi.org/10.1016/j.jenvman.2012.10.061

Zhou, D., Wang, Y., Memon, M.Z., Fu, W., Wu, Z., Sheng, S., Zhang, H., Ji, G., The Effect of Na2ZrO3 Synthesis Method on the CO2 Sorption Kinetics at High Temperature. Carbon Capture Science & Technology 3, 100050. 2022. https://doi.org/10.1016/j.ccst.2022.100050